Batteries & Supercaps

Concept
doi.org/10.1002/batt.202100207

Chemistry Europe
European Chemical Societies Publishing

www.batteries-supercaps.org

VIP *Very Important Paper*

Special Collection

Guiding Uniform Sodium Deposition through Host Modification for Sodium Metal Batteries

Chhail Bihari Soni,[a] Vipin Kumar,*[a, b] and Zhi Wei Seh*[c]

Room-temperature Na metal batteries represent an emerging energy storage technology beyond Li-ion batteries, owing to the high specific capacity and high natural abundance of Na. However, Na metal anodes are plagued with multiple challenges including unstable solid electrolyte interphase, undesirable dendrite growth, and large volumetric expansion, leading to low Coulombic efficiency during Na plating and stripping. To this end, mechanically stable and sodiophilic hosts with nano- or micro-structured materials have been investigated to accommodate Na in the structured spacing or gaps for enhanced cyclability. In this concept, we will discuss the key concepts and latest developments in guiding uniform Na deposition through host modification, especially carbon, inorganic and polymeric materials. Future prospects and outlook will also be provided, including artificial interphase design, solid-state electrolytes, and precise nanoscale characterization to improve our fundamental understanding of Na deposition and spur this burgeoning field in Na metal batteries.

1. Introduction

The quest towards sustainable but intermittent renewable energy sources (such as solar and wind) warrants the need for advanced energy storage technologies to provide power on demand.[1] To this end, many researchers have begun the search for new rechargeable battery technologies beyond conventional Li-ion intercalation chemistry.[2] Room-temperature Na metal batteries are one of the most compelling candidates due to the high specific capacity of Na metal anode,[3] in addition to its high elemental abundance in the Earth's crust.[4] Room-temperature Na metal batteries work based on repeated Na deposition and dissolution, unlike the typical intercalation chemistry in Li-ion batteries. This drastically different battery chemistry results in much higher theoretical specific capacity of Na metal anode (1,166 mAh g^{-1}) compared to typical graphite anode (372 mAh g^{-1}).[5]

Moreover, operating Na metal batteries such as Na–S chemistry at room temperature, leads to improved safety characteristics compared to their high-temperature Na–S counterparts, which typically operate at 300 to 350 °C using molten Na anode.[3a] Room-temperature Na–S batteries also enable complete discharge of S_8 to Na_2S, unlike their high-temperature analogues which allow only partial discharge to molten Na_2S_3, because further discharge will cause solid Na_2S_2 and Na_2S to precipitate out.[6] This gives room-temperature Na–S batteries a much higher specific energy of 1,274 Wh kg^{-1} compared to 760 Wh kg^{-1} for high-temperature Na–S batteries.[3e] Apart from Na–S batteries, Na-air batteries are gaining immense attention as well because of their high specific energy (~1,605 Wh kg^{-1})[7] and low cost (projected to be 1/3rd of Li-air batteries).[8] The technology of room-temperature Na–S and Na-air batteries is still in its infancy, and demands much more research to realize its full potential.

In the field of room-temperature Na metal batteries, many crucial problems remain unresolved with regards to the Na metal anode.[9] Ideally, the Na metal surface should be protected by a uniform and compact solid electrolyte interphase (SEI) that conducts Na^+ and prevents further reaction with the electrolyte.[10] However, typical non-uniform and porous SEIs expose highly reactive Na metal which reacts continuously with the electrolyte, leading to low Coulombic efficiency during Na plating and stripping.[11] Non-uniform Na^+ flux also results in Na dendrite growth and constant breaking and reforming of the SEI, causing eventual battery failure due to fast electrolyte depletion and high SEI resistance.[12] Dendrites that break off from the Na metal anode can also become "dead Na", leading to loss of electrical contact and active material.[13] Moreover, dendrites can penetrate the separator and cause serious short circuits which is a major safety concern. Volume change of the Na metal anode, which is virtually infinite in the case of metal anode batteries, has recently received immense attention as well. Large volumetric expansion can result in mechanical instability of the SEI and formation of cracks, resulting in poor reversibility of Na metal anodes.[14]

To address the aforementioned issues, mechanically stable hosts with nano-or micro-structured materials have been explored to accommodate Na in the structured spacing or

[a] C. B. Soni, Prof. V. Kumar
Department of Energy Science and Engineering
Indian Institute of Technology Delhi
Hauz Khas, New Delhi, 110016, India
E-mail: vkumar@ces.iitd.ac.in
[b] Prof. V. Kumar
University of Queensland – IIT Delhi Academy of Research (UQIDAR)
Indian Institute of Technology Delhi
Hauz Khas, New Delhi, 110016, India
[c] Prof. Z. W. Seh
Institute of Materials Research and Engineering
Agency for Science, Technology and Research (A*STAR)
2 Fusionopolis Way, Innovis, 138634, Singapore
E-mail: sehzw@imre.a-star.edu.sg

Special Collection An invited contribution to a joint Special Collection between – ChemElecroChem and Batteries & Supercaps dedicated to research Beyond Lithium-Ion Batteries.

gaps.[15] These host materials were found to enable homogeneous Na deposition, hence improving the Coulombic efficiency and cyclability of Na metal anodes.[16] In this concept, we will discuss the general concepts and important developments in guiding uniform Na deposition through host modification. In addition, we also propose future research directions, including artificial interphase design, solid-state electrolytes, and accurate nanoscale characterization. The overall structure of the article is summarized in the schematics in Figure 1.

2. Guiding Na Deposition through Host Modification

Ideal host materials for Na deposition should possess the following characteristics: 1) robust mechanical properties to suppress dendrite formation,[17] 2) excellent wettability (or sodiophilicity) to promote uniform Na deposition,[18] 3) large internal spacing or porosity to accommodate volume change, and 4) low cost and ease of fabrication for practical applications. As a result, carbon materials are among the most popular host choices so far due to their combination of the above attributes.

Inspired from the sodiophilic properties of reduced graphene oxide (rGO), Wang *et al.*[19] designed processable and moldable Na metal anodes by simply contacting rGO on molten Na, with Na being drawn between the inter-layer spacing by capillary effect. The composite could also be designed in various shapes and sizes, such as 1D nanofibers, 2D films, and 3D monoliths, see Figure 2(a). Na/rGO composites with only 4.5 wt.% rGO exhibited greatly enhanced hardness, strength, and stability against environmental corrosion compared to pure Na. The stripping/plating of Na can be significantly extended in both ether and carbonate electrolytes with extremely low polarization at all current densities (1–5 mA cm^{-2}). Apparent advantages of this approach include: 1) volume changes being potentially minimized by dividing Na deposition into smaller domain regions, 2) propensity for Na dendrites can be greatly reduced due to homogeneous deposition, and 3) interlayer region acting as a buffer to accommodate fluctuating stress levels, thus improving safety.

To further improve accommodation capacity and wettability, Wu *et al.*[20] used a modified hydrothermal reduction reaction and subsequent oriented freeze-drying process to design a reduced graphene oxide aerogel (rGa), see Figure 2(b). The rGa host was identified to have abundant oxygen functional groups [Figure 2(c)] which helped improve Na wettability, and oriented freeze-drying ensuring a highly homogeneous pore structure. Owing to its unique structural and chemical properties, the encapsulated composite anode showed an ultra-high loading of Na metal at 98.75 wt.%, and could be cycled for over 400 h at 5 mA cm^{-2}.

Zheng *et al.*[21] proposed oxygen-nitrogen co-doped graphitized carbon fibers (DGCF) with uniformly distributed sodiophilic sites (–COOR, –C=O, and –OH), see Figure 2(d, e), as a host to accommodate large volume changes upon cycling. First principles calculations were conducted to understand the

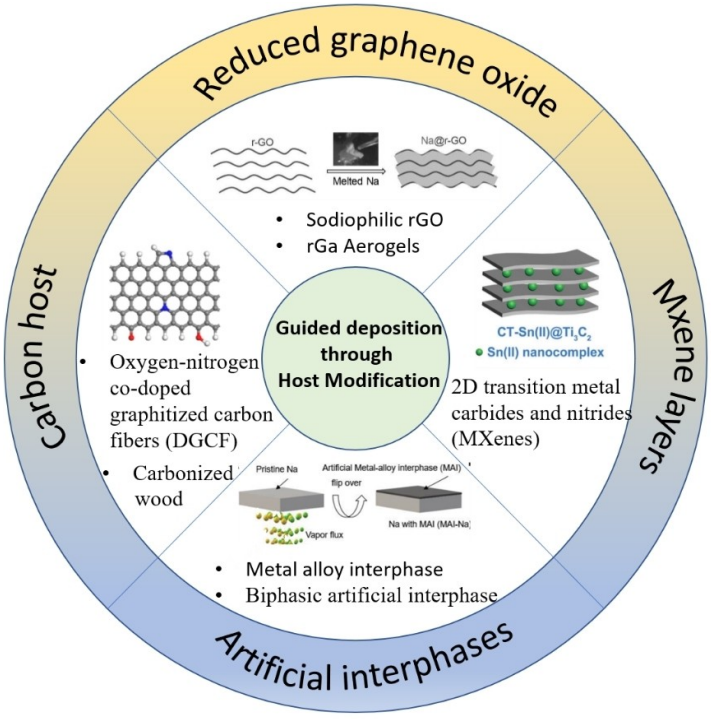

Figure 1. Summary of the Na host modification strategies covered in this article. Reproduced from Ref. [19] with permission. Copyright (2017) Wiley-VCH Verlag GmbH & Co. KGaA, Weinheim. Reproduced from Ref. [21] with permission. Copyright (2018) American Chemical Society. Reproduced from Ref. [24] with permission. Copyright (2019) Wiley-VCH Verlag GmbH & Co. KGaA, Weinheim. Reproduced from Ref. [27] with permission. Copyright (2020) Elsevier.

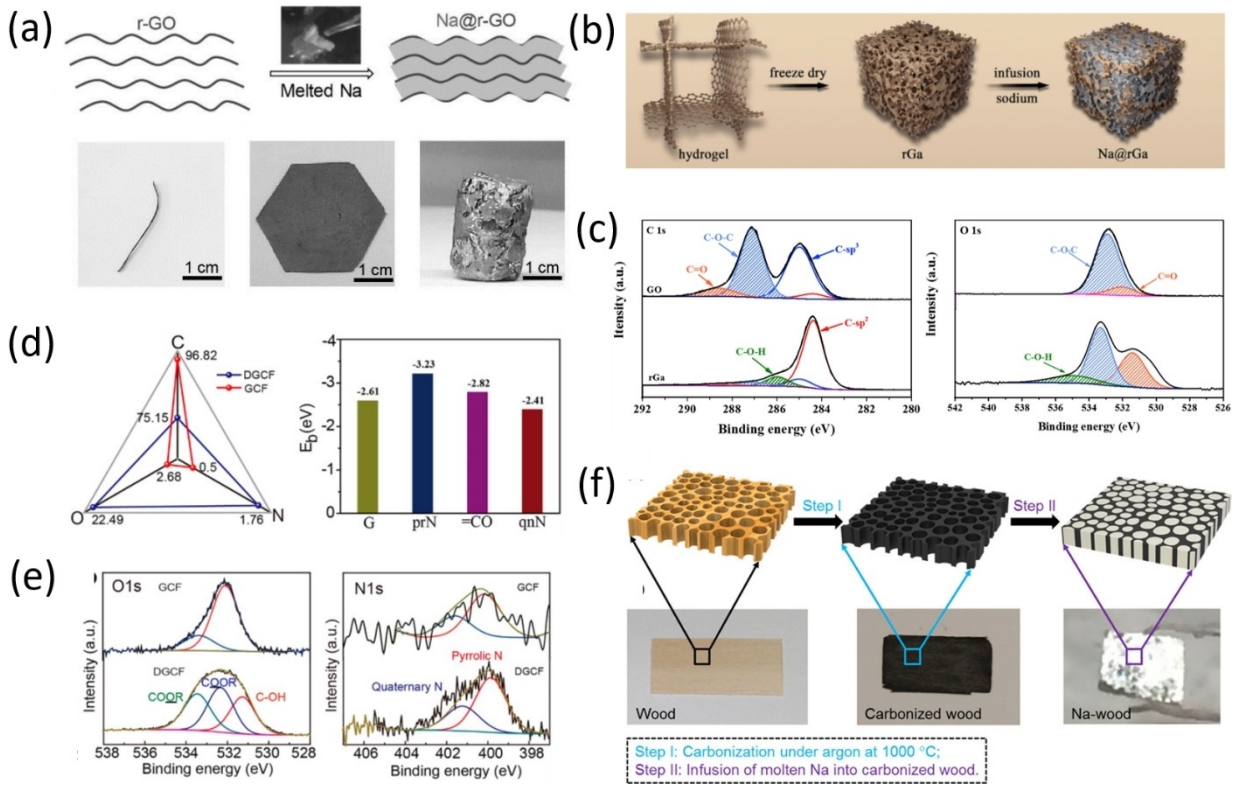

Figure 2. (a) Schematic representing the fabrication of Na@r-GO composites. Closely packed GO films can swell due to the gas evolved during the reduction reaction. Upon contacting with r-GO, the melted Na can be absorbed into the gap among the r-GO sheets. Optical images show moldable 1D, 2D and 3D shapes of composite. Reproduced from Ref. [19] with permission. Copyright (2017) Wiley-VCH Verlag GmbH & Co. KGaA, Weinheim. (b) Synthetic representation of Na@rGa composite anode: rGO hydrogel→rGa→Na@rGa composite sample, (c) X-ray photoelectron spectroscopy (XPS) spectra of C 1s and O 1s of GO film and rGa-4h sample respectively. Reproduced from Ref. [20] with permission. Copyright (2019) Elsevier. (d) Atomic concentration comparison of N, O, and C and binding energy of a Na atom with different functional groups of DGCF, (e) XPS spectra of bare GCF and DGCF for O 1s and N 1s. Reproduced from Ref. [21] with permission. Copyright (2018) American Chemical Society. (f) Encapsulation of metallic Na into carbonized wood by a spontaneous and instantaneous infusion (5 seconds). Reproduced with permission from Ref. [22]. Copyright (2017) American Chemical Society.

binding interactions of the various sites with Na. The assembled Na-DGCF symmetric cells could be cycled for over 1200 hours at relatively high current density (3 mA cm^{-2}). Zhang *et al.*[23] reported a composite 3D multilayer host for thermally pre-storing Na or Li metal. Since pristine carbon nanofibers (CNF) show poor affinity towards molten Na or Li, the wettability was improved by conformally decorating SnO_2 over CNF by hydrothermal reaction. Exploiting the strong affinity of Sn towards alkali metals, melt infusion of Na or Li could be achieved in a few seconds, though the loading remains low at ~52% compared to rGa.

Unlike most artificial carbon hosts, naturally occurring carbonized wood consists of orderly distributed micro/nano-sized channels, which can be easily accessed by ions or molten Na through the capillary effect. Na deposits can then be restrained inside, with the high surface area of the carbonized host inhibiting volume changes during stripping/plating. Recently, Luo *et al.*[22] demonstrated a strategy to encapsulate Na metal through melt infusion (~5 sec) into an electrically conductive matrix with a porous channel structure, see Figure 2(f). The engineered Na electrode exhibited stable stripping/plating for over 250 cycles compared to pristine Na which could sustain only 90 cycles.

Besides carbon materials, other inorganic materials have also been explored as potential host candidates to accommodate Na deposits, such as 2D transition metal carbides and nitrides (MXenes). In this regard, Luo *et al.*[24] demonstrated Sn^{2+} pillared Ti_3C_2 MXenes as a stable matrix for dendrite-free Na deposition. The Sn-based complexes located within the MXene layers were found to guide Na nucleation and growth within the interlayer spaces, resulting in uniform deposition of Na. In the process, $Na_{15}Sn_4$ alloy was formed, which allowed Na to continue depositing within the MXene layers due to the "pillar effect". As a result, the pillared MXene-based Na electrode could cycle up to 500 cycles at a current density of 4 mA cm^{-2} and areal capacity of 4 mAh cm^{-2}. A follow up work by the same group reported a novel 1D/2D $Na_3Ti_5O_{12}$-MXene hybrid nanostructure,[25] consisting of $Na_3Ti_5O_{12}$ nanowires synthesized between Ti_3C_2 MXene nanosheets, for use as a matrix for controlled Na deposition, see Figure 3. Stable Na anode cycling performance was attained at a high current density up to 10 mA cm^{-2}, together with a very high areal capacity up to 20 mAh cm^{-2}.

Owing to the host-less nature of Na, it is very difficult to confine the Na dendrite growth and volume change, and so elastic polymeric materials have been explored as hosts. Li and

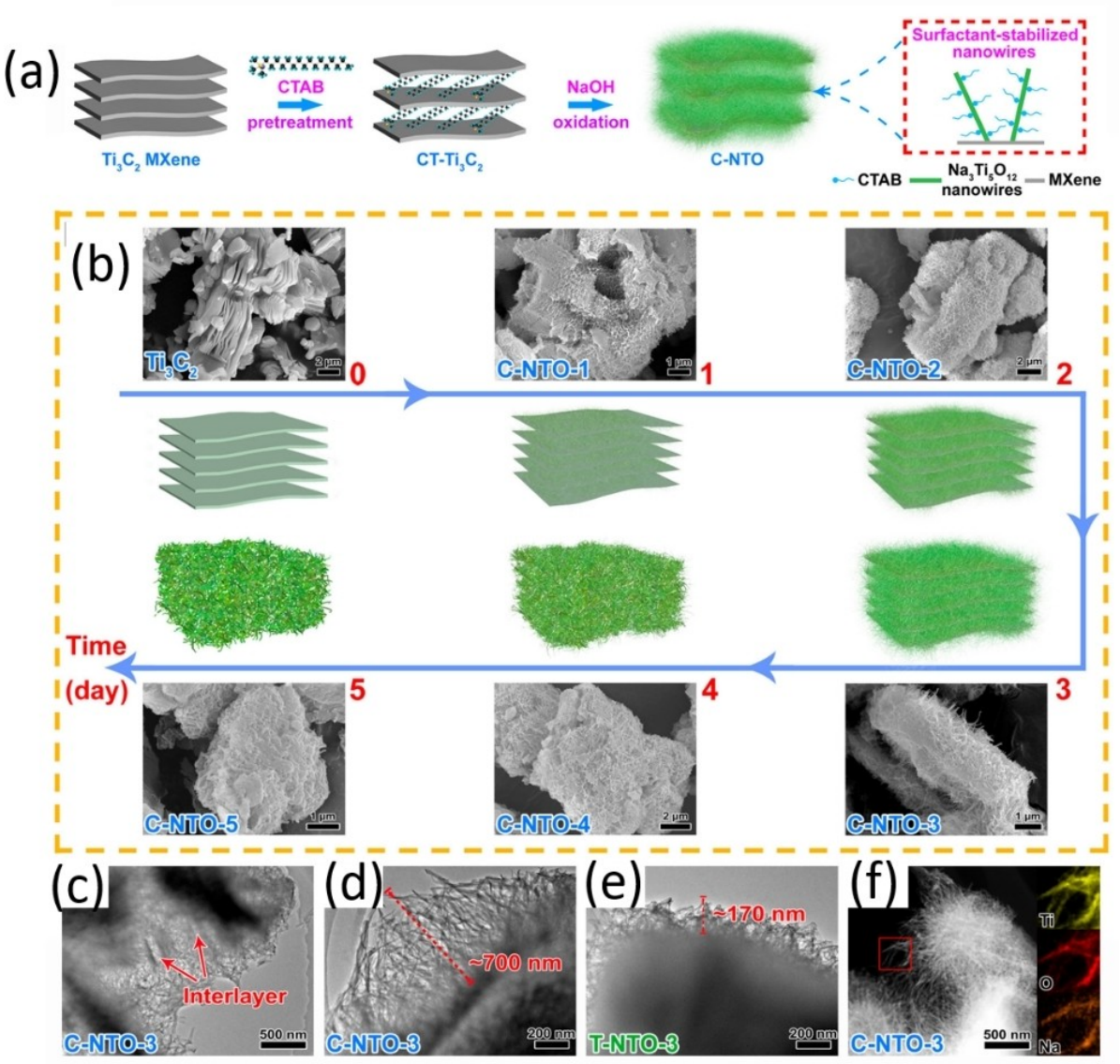

Figure 3. (a) Schematic illustration of the preparation of CT-Ti_3C_2-derived 1D/2D $Na_3Ti_5O_{12}$-MXene hybrid nanoarchitecture (C-NTO). (b) Schematic illustrating the morphology evolution of C-NTO during the oxidation process and the corresponding SEM images of Ti_3C_2, C-NTO-1, C-NTO-2, C-NTO-3, C-NTO-4, and C-NTO-5. TEM images of (c, d) C-NTO-3, (e) Ti_3C_2-derived T-NTO-3. (f) Scanning TEM image of C-NTO-3, and elemental mappings of Ti, O, and Na (insets). Reproduced from Ref. [25] with permission. Copyright (2020) American Chemical Society.

co-workers[26] used an insulating scaffold i.e., polyacrylonitrile (PAN) as 3D host for Na metal. Due to the porous nature of the host, it is believed to regulate current density that may lead to curtailing dendrite growth. Since PAN exhibits sodiophilic properties, it enables the homogeneous distribution of Na ions, and the presence of Sn atoms further facilitates smooth and dense Na deposition. The resulting Na metal anode could be cycled for over 2500 h at 2 mA cm^{-2}. Exploration of other non-carbon host materials with sodiophilic sites and co-doping will open up new opportunities in this burgeoning field of research.

3. Prospects and Outlook

A promising future research direction is to combine Na host modification with artificial interphase design to further stabilize Na deposition. Artificial interphases need to possess high ionic conductivity to facilitate fast Na diffusion, high Young's modulus (stiffness) to suppress undesirable dendrite growth, and high critical strain (ductility) to accommodate large volumetric expansion. Recently, Kumar *et al.*[27] demonstrated a metal alloy artificial interphase ($Na_{1.17}Sn_2$) on Na anode that combines these properties [Figure 4(a)]. The interphase was found to enable fast Na^+ transport kinetics and dendrite-free Na growth, allowing reversible Na plating and stripping at current densities up to 7 mA cm^{-2} in a symmetric cell configuration. As a follow up work, the authors further demonstrated

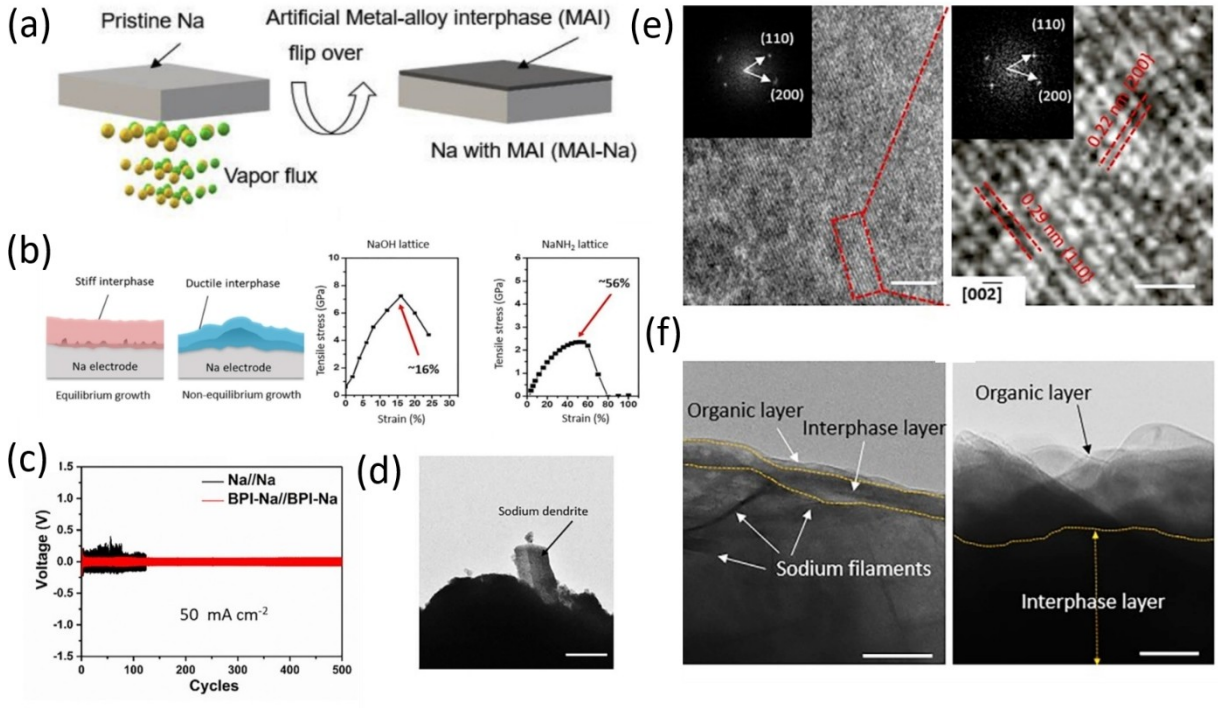

Figure 4. (a) Schematic illustration of the process steps involved in the formation of the interphase. Reproduced from Ref. [27] with permission. Copyright (2020) Elsevier. (b) Schematic representation of the interphases on the Na electrode, depicting the suppression of large dendrite formation (due to stiff NaOH interphase) and accommodation of large volumetric expansion (due to ductile $NaNH_2$ interphase) during Na growth, as well as stress-strain curve of NaOH and $NaNH_2$. (c) Galvanostatic cycling of Na in symmetric cell configurations with and without BPI at 50 mA cm^{-2} current density and 1 mAh cm^{-2} capacity. (d) Cryo-TEM image of Na dendrite grown on the grid (scale bar, 1 nm). (e) High-resolution cryo-TEM images of the Na dendrite; inset shows a corresponding fast Fourier transform (FFT) image (scale bar, 5 nm) and enlarged view of the selected region (scale bar, 1 nm). (f) Cryo-TEM cross-sectional images of Na deposition with BPI at rotation 25° (scale bar, 50 nm) and rotation 30° (scale bar, 10 nm), respectively. Reproduced from Ref. [28] with permission. Copyright (2020) Elsevier.

a biphasic interphase (BPI)[28] on Na anode comprising NaOH and $NaNH_2$ [Figure 4(b)], which could cycle reversibly even at a very high current density of 50 mA cm^{-2} [Figure 4(c)]. The synergistic combination of artificial interphase design and Na host modification will pave the way for the development of high-performance Na metal batteries.

Moreover, we also propose to combine Na host modification with solid-state electrolytes, such as solid polymer electrolytes (SPEs), which have better thermal stability and resistance against dendrite growth compared to liquid electrolytes.[31] An ideal SPE should have good ionic conductivity, high interfacial stability, low interfacial resistance, poor electrical conductivity, and excellent thermo-mechanical integrity.[32,33] Since the seminal work of Parker and Wright on SPEs that unveiled the ability of poly(ethylene oxide) (PEO) to solvate high concentrations of alkali metal ions (*e.g.*, Na and K), PEO has been a popular choice as polymer hosts.[34] For example, West *et al.*[35] and Hashmi *et al.*[36] studied the interface stabilities of PEO-$NaClO_4$ and PEO-$NaPF_6$ in all-solid-state cells at 80 °C, with special emphases given to the compatibility between the polymers and metallic Na, and their corresponding interface stabilities. Besides PEO which often exists in the ring configuration and known to have better diffusive properties, other linear-chain polymers such as polyvinyl alcohol (PVA) and polyvinylpyrrolidone (PVP) have been investigated for Na^+ ion conduction. The addition of small amounts of plasticizers may also enhance their ionic transport. Chandrasekaran *et al.*[29] added low molecular weight polyethylene glycol (PEG) (~4000 g mol^{-1}) to PEO-$NaClO_3$ as a means to repair the interfacial layer over the Na surface, and reported an improvement in ionic conductivity by ~10^3, see Figure 5(a). Another alternative approach is the design of cross-linked network SPEs. Zheng *et al.*[30] designed a hybrid SPE by cross-linking amine-terminated PEG with octakis (3-glycidyloxypropyldimethylsiloxy) octasilsesquioxane (octa-POSS) containing $NaClO_4$. Migration of the SEI into the SPE was reported for the first time, attributed to the mechanical softness and reactivity of Na metal, see Figure 5(b, c). Symmetric Na cells demonstrated stable function at 80 °C for over 3550 hours at a current density of 0.5 mA cm^{-2}. Besides SPEs, other solid-state electrolytes such as inorganic superionic conductors and ceramic/polymer composites may also be explored.

In addition, accurate nanoscale characterization of Na deposition is also of paramount importance. Alkali metals such as Na are highly beam-sensitive, hence cryogenic transmission electron microscopy (cryo-TEM) has recently emerged to study such materials while preserving their structural and electrochemical stability. In this respect, Kumar *et al.*[27,28] reported a cryo-TEM study of Na dendrites [Figure 4(d)], where the observed lattice fringes of about 0.22 nm and 0.29 nm, which correspond to the (200) and (110) planes of Na respectively, indicate the crystalline nature of the Na dendrites, see Fig-

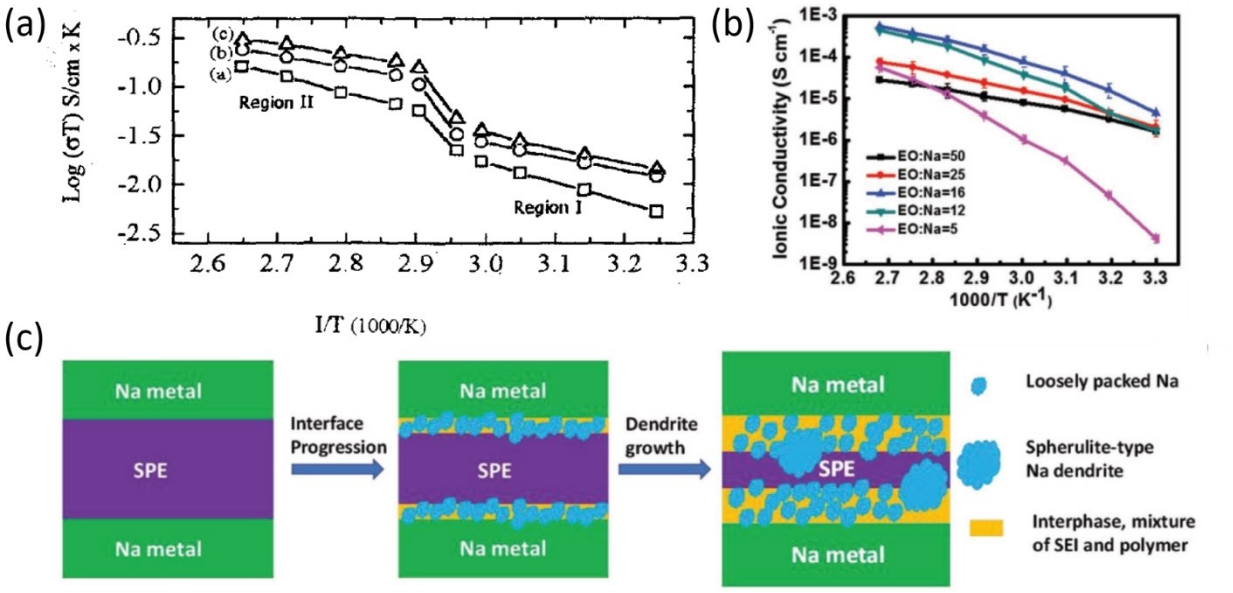

Figure 5. (a) Inverse temperature vs. conductivity curves for a) PEG + PEO + $NaClO_3$ (30% + 60% + 10%) + PC (10%), b) PEG + PEO + $NaClO_3$ (45% + 45% + 10%) + PC (10%), c) PEG + PEO + $NaClO_3$ (60% + 30% + 10%) + PC (10%). Reproduced from Ref. [29] with permission. Copyright (2001) Springer Nature. (b) Ionic conductivity of different SPEs as a function of temperature (EO: ethylene oxide). (c) Schematic of the evolution and migration of the Na | SPE interface under symmetric cell cycling. Reproduced from Ref. [30] with permission. Copyright (2018) WILEY-VCH Verlag GmbH & Co. KGaA, Weinheim.

ure 4(e,f). The growth direction of the dendrites was identified to be along $<00\bar{2}>$, which could be due to the relatively low surface energy along this direction. Future studies should seek to further quantify the relative abundance of other growth directions to fully understand the process of Na deposition and dendrite formation in host materials. This can be complemented with theoretical computations such as molecular dynamics simulations to model the deposition behavior of Na under different cycling conditions.

On a related note, Cui and co-workers[37] also conducted cryo-TEM studies on a cycled Li metal anode to examine the growth of Li dendrites. They observed that Li metal dendrites grow as single-crystalline nanowires along different directions [Figure 6(a)] primarily along $<111>$, $<110>$ and $<211>$, where $<111>$ was noticed as the perferred growth direction (about 49% of dendrites follow the same) in liquid carbonate-based electrolyte system. It is noteworthy that dendrite growth direction may vary at kinks without a noticeable crystal defect. For instance, Figure 6(a) shows the Li dendrite growth direction changing between $<211>$ and $<110>$ at the first kink and then switched to $<211>$ at the second kink, which might correspond to the stalking faults or twin boundaries. Moreover, in a separate contribution, they examined the effect of temperature on the structure of Li dendrites.[38] It was observed that with an increase in temperature, the lateral size of the Li dendrites increases linearly. Besides that, SEI layer thickness was found to be sensitive to temperature change, see Figure 6(b). Kourkoutis and co-workers[39] also examined the growth pattern of Li dendrites through cryogenic scanning transmission electron microscopy (cryo-STEM) and focused ion beam techniques. They unveiled two types of dendrites (e.g., type I and type II) in Figure 6(c), that can grow on the Li anode with distinct chemical composition and physical structure. Type I dendrites were about 5 μm with low lateral expansion, whereas type II dendrites were about 100–300 nm thick and had tortuous morphology. Due to the delicate nature of type II dendrites, they were found susceptible to disconnect with the electrode during battery operation, causing loss of Li metal inventory. Though we have gained some fundamental understanding of alkali metal dendrites, more investigations are needed to provide insight on the growth behaviour of alkali metals at defect sites or under variable temperature conditions.

Despite several reports on Na dendrite formation and growth, they still lack a basic understanding on the effect of surface roughness and local current density distribution. For instance, it was believed that a rough Na metal surface promotes random distribution of ion flux that forms dendrites and a non-uniform SEI.[5] Contrary to this, some reports claimed that an uneven geometrical surface does not contribute significantly to the generation of dendrites since SEI is intrinsically heterogeneous.[41] Zheng and co-workers[40] studied in-situ electrochemical liquid cell TEM to examine the electrochemical deposition of Na. The growth dynamics of Na deposition were investigated over both flat [Figure 6(d,e)] and curved [Figure 6(f)] Ti surfaces. On a flat surface, rapid Na deposition was observed without apparent formation of Na grains, and the deposition was observed to slow down when the SEI thickness reached 130 nm. Contrary to this, Na grains emerged on the sharp curvature and grew into various agglomerates.

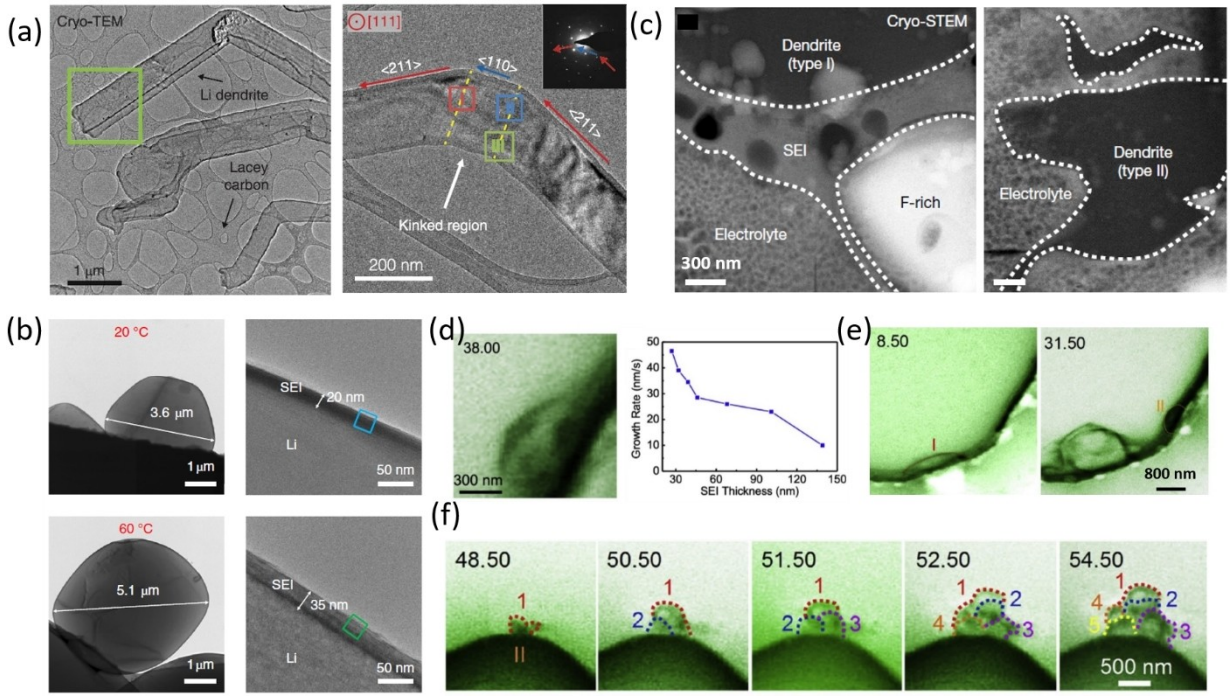

Figure 6. (a) Cryo-TEM image of Li metal dendrites. Electron dose rate < 1 e Å^{-2} s^{-1} and TEM image of kinked Li metal dendrite that changes from a $< 211 >$ to $< 110 >$ and back to $< 211 >$ growth direction. The dashed yellow lines indicate a change in the growth direction. Reproduced from Ref. [37] with permission. Copyright (2017) The American Association for the Advancement of Science. (b) Cryo-TEM reveals an emergent SEI nanostructure formed at elevated temperature, 20 °C and 60 °C. The cryo-TEM images of Li metal particles show the particle size and cryo-TEM images of the SEI interface show the SEI thickness. Reproduced from Ref. [38] with permission. Copyright (2019) Springer Nature. (c) High-angle annular dark-field cryo-STEM imaging shows an extended SEI layer on the type I dendrite but not on the type II dendrite. Reproduced from Ref. [39] with permission. Copyright (2018) Springer Nature. (d) Na grain growth rate versus SEI thickness. (e) Sequential TEM images show the nucleation and growth of Na grains under a negative potential on a flat Ti electrode. (f) The initial deposition of Na grains on a nodule of Ti electrode with high curvature shows the base growth behaviour. Reproduced from Ref. [40] with permission. Copyright (2020) Elsevier.

4. Conclusions

In summary, guiding Na deposition through host modification is a promising strategy to spur the development of highly reversible Na metal anodes. The combination of artificial interphase design, solid-state electrolytes, and precise nano-scale characterization is expected to advance our fundamental understanding of Na deposition and provide new avenues for the progress of Na metal batteries. These insights can be extended to other rechargeable battery technologies such as multivalent Mg and Zn metal batteries as well.

Acknowledgements

C. B. S. acknowledges the scholarship awarded by the Indian Institute of Technology Delhi (IIT Delhi). This work was financially supported by the IIT Delhi and the Singapore National Research Foundation (NRF-NRFF2017-04).

Conflict of Interest

The authors declare no conflict of interest.

Keywords: carbon host · dendrites · sodiophilic · sodium anode · solid electrolyte interphase

[1] a) G. Papaefthymiou, K. Dragoon, *Energy Policy* **2016**, *92*, 69–82; b) J. Liu, J. Wang, C. Xu, H. Jiang, C. Li, L. Zhang, J. Lin, Z. X. Shen, *Adv. Sci.* **2018**, *5*, 1700322; c) J.-M. Ma, Y.-T. Li, *Rare Met.* **2021**, *40*, 246–248.
[2] a) K. Kubota, M. Dahbi, T. Hosaka, S. Kumakura, S. Komaba, *Chem. Rec.* **2018**, *18*, 459–479; b) R. Usiskin, Y. Lu, J. Popovic, M. Law, P. Balaya, Y.-S. Hu, J. Maier, *Nat. Rev. Mater.* **2021**, DOI: 10.1038/s41578-021-00324-w.
[3] a) C. B. Soni, Sungjemmenla, S. Vineeth, V. Kumar, *Energy Storage.* **2021**, e264, DOI: 10.1002/est2.264; b) Y. Zhao, K. R. Adair, X. Sun, *Energy Environ. Sci.* **2018**, *11*, 2673–2695; c) Y. Wang, Y. Zhang, H. Cheng, Z. Ni, Y. Wang, G. Xia, X. Li, X. Zeng, *Molecules* **2021**, *26*, 1535; d) S. Zhang, Y. Yao, Y. Yu, *ACS Energy Lett.* **2021**, *6*, 529–536; e) Y. X. Wang, B. Zhang, W. Lai, Y. Xu, S. L. Chou, H. K. Liu, S. X. Dou, *Adv. Energy Mater.* **2017**, *7*, 1602829.
[4] Y. Wang, D. Zhou, V. Palomares, D. Shanmukaraj, B. Sun, X. Tang, C. Wang, M. Armand, T. Rojo, G. Wang, *Energy Environ. Sci.* **2020**, *13*, 3848–3879.
[5] B. Lee, E. Paek, D. Mitlin, S. W. Lee, *Chem. Rev.* **2019**, *119*, 5416–5460.
[6] C. B. Soni, S. Vineeth, V. Kumar, *Materials Today Advances* **2021**, *2*, 4165–4189.
[7] a) Z. W. Seh, J. Sun, Y. Sun, Y. Cui, *ACS Cent. Sci.* **2015**, *1*, 449–455; b) C. Li, M. Qiu, R. Li, X. Li, M. Wang, J. He, G. Lin, L. Xiao, Q. Qian, Q. Chen, J. Wu, X. Li, Y.-W. Mai, Y. Chen, *Adv. Fiber Mater.* **2021**, DOI: 10.1007/s42765-021-00088-6.
[8] X. Liu, X. Lei, Y.-G. Wang, Y. Ding, *ACS Cent. Sci.* **2021**, *7*, 335–344.
[9] X. Zheng, C. Bommier, W. Luo, L. Jiang, Y. Hao, Y. Huang, *Energy Storage Mater.* **2019**, *16*, 6–23.

[10] A. Y. S. Eng, V. Kumar, Y. Zhang, J. Luo, W. Wang, Y. Sun, W. Li, Z. W. Seh, *Adv. Energy Mater.* **2021**, *11*, 2003493.
[11] L. Fan, X. Li, *Nano Energy* **2018**, *53*, 630–642.
[12] A. Hagopian, M.-L. Doublet, J.-S. Filhol, *Energy Environ. Sci.* **2020**, *13*, 5186–5197.
[13] W. Liu, P. Liu, D. Mitlin, *Chem. Soc. Rev.* **2020**, *49*, 7284–7300.
[14] Y. Zhao, X. Yang, L. Y. Kuo, P. Kaghazchi, Q. Sun, J. Liang, B. Wang, A. Lushington, R. Li, H. Zhang, *Small* **2018**, *14*, 1703717.
[15] a) Q. Lu, X. Wang, A. Omar, D. Mikhailova, *Mater. Lett.* **2020**, *275*, 128206; b) C. Bao, B. Wang, Y. Xie, R. Song, Y. Jiang, Y. Ning, F. Wang, T. Ruan, D. Wang, Y. Zhou, *ACS Sustainable Chem. Eng.* **2020**, *8*, 5452–5463.
[16] J. Xia, F. Zhang, J. Liang, K. Fang, W. Wu, X. Wu, *J. Alloys Compd.* **2021**, *853*, 157371.
[17] a) S. S. Chi, X. G. Qi, Y. S. Hu, L. Z. Fan, *Adv. Energy Mater.* **2018**, *8*, 1702764; b) J. Zhang, W. Wang, R. Shi, W. Wang, S. Wang, F. Kang, B. Li, *Carbon* **2019**, *155*, 50–55.
[18] M. Zhu, S. Li, B. Li, Y. Gong, Z. Du, S. Yang, *Sci. Adv.* **2019**, *5*, eaau6264.
[19] A. Wang, X. Hu, H. Tang, C. Zhang, S. Liu, Y. W. Yang, Q. H. Yang, J. Luo, *Angew. Chem.* **2017**, *129*, 12083–12088.
[20] F. Wu, J. Zhou, R. Luo, Y. Huang, Y. Mei, M. Xie, R. Chen, *Energy Storage Mater.* **2019**, *22*, 376–383.
[21] Z. Zheng, X. Zeng, H. Ye, F. Cao, Z. Wang, *ACS Appl. Mater. Interfaces* **2018**, *10*, 30417–30425.
[22] W. Luo, Y. Zhang, S. Xu, J. Dai, E. Hitz, Y. Li, C. Yang, C. Chen, B. Liu, L. Hu, *Nano Lett.* **2017**, *17*, 3792–3797.
[23] X. Zhang, J. Liang, G. Gao, S. Ding, Z. Yang, W. Yu, B. Q. Li, *Electrochim. Acta* **2013**, *98*, 263–267.
[24] J. Luo, C. Wang, H. Wang, X. Hu, E. Matios, X. Lu, W. Zhang, X. Tao, W. Li, *Adv. Funct. Mater.* **2019**, *29*, 1805946.
[25] J. Luo, X. Lu, E. Matios, C. Wang, H. Wang, Y. Zhang, X. Hu, W. Li, *Nano Lett.* **2020**, *20*, 7700–7708.
[26] Y. Xu, C. Wang, E. Matios, J. Luo, X. Hu, Q. Yue, Y. Kang, W. Li, *Adv. Energy Mater.* **2020**, *10*, 2002308.
[27] V. Kumar, A. Y. S. Eng, Y. Wang, D.-T. Nguyen, M.-F. Ng, Z. W. Seh, *Energy Storage Mater.* **2020**, *29*, 1–8.
[28] V. Kumar, Y. Wang, A. Y. S. Eng, M.-F. Ng, Z. W. Seh, *Cell Rep. Phys. Sci.* **2020**, *1*, 100044.
[29] R. Chandrasekaran, I. Ruth Mangani, R. Vasanthi, S. Selladurai, *Ionics* **2001**, *7*, 94–100.
[30] Y. Zheng, Q. Pan, M. Clites, B. W. Byles, E. Pomerantseva, C. Y. Li, *Adv. Energy Mater.* **2018**, *8*, 1801885.
[31] Y. Lu, L. Li, Q. Zhang, Z. Niu, J. Chen, *Joule* **2018**, *2*, 1747–1770.
[32] X. Li, W. Chen, Q. Qian, H. Huang, Y. Chen, Z. Wang, Q. Chen, J. Yang, J. Li, Y. W. Mai, *Adv. Energy Mater.* **2021**, *11*, 2000845.
[33] Y. Chen, Z. Wang, X. Li, X. Yao, C. Wang, Y. Li, W. Xue, D. Yu, S. Y. Kim, F. Yang, A. Kushima, G. Zhang, H. Huang, N. Wu, Y.-W. Mai, J. B. Goodenough, J. Li, *Nature* **2020**, *578*, 251–255.
[34] a) D. E. Fenton, J. M. Parker, P. V. Wright, *Polymer* **1973**, *14*, 589; b) P. V. Wright, *Electrochim. Acta* **1998**, *43*, 1137–1143.
[35] K. West, B. Zachau-Christiansen, T. Jacobsen, S. Skaarup, *J. Power Sources* **1989**, *26*, 341–345.
[36] S. A. Hashmi, S. Chandra, *Mater. Sci. Eng. B* **1995**, *34*, 18–26.
[37] Y. Li, Y. Li, A. Pei, K. Yan, Y. Sun, C.-L. Wu, L.-M. Joubert, R. Chin, A. L. Koh, Y. Yu, J. Perrino, B. Butz, S. Chu, Y. Cui, *Science* **2017**, *358*, 506–510.
[38] J. Wang, W. Huang, A. Pei, Y. Li, F. Shi, X. Yu, Y. Cui, *Nat. Energy* **2019**, *4*, 664–670.
[39] M. J. Zachman, Z. Tu, S. Choudhury, L. A. Archer, L. F. Kourkoutis, *Nature* **2018**, *560*, 345–349.
[40] Z. Zeng, P. Barai, S.-Y. Lee, J. Yang, X. Zhang, W. Zheng, Y.-S. Liu, K. C. Bustillo, P. Ercius, J. Guo, Y. Cui, V. Srinivasan, H. Zheng, *Nano Energy* **2020**, *72*, 104721.
[41] S. Shi, P. Lu, Z. Liu, Y. Qi, L. G. Hector Jr, H. Li, S. J. Harris, *J. Am. Chem. Soc.* **2012**, *134*, 15476–15487.

Manuscript received: August 10, 2021
Revised manuscript received: September 14, 2021
Accepted manuscript online: September 15, 2021
Version of record online: October 4, 2021